

# Experimental Validation of Wave Induced Disturbances for Predictive Station Keeping of a Remotely Operated Vehicle

Kyle L. Walker<sup>1</sup> , *Student Member, IEEE*, Roman Gabl<sup>2,3</sup> , Simona Aracri<sup>1,4</sup> , Yu Cao<sup>3</sup> , *Member, IEEE*, Adam A. Stokes<sup>1</sup> , *Member, IEEE*, Aristides Kiprakis<sup>3</sup> , *Senior Member, IEEE*, Francesco Giorgio-Serchi<sup>1</sup> 

**Abstract**—Predictive control methods can substantially improve the performance of Unmanned Underwater Vehicles (UUVs), particularly in shallow water environments or near the free surface where wave induced disturbance are of magnitude comparable to the vehicle characteristic inertia. To facilitate the adoption of these methods, a fast estimation of the time evolution of hydrodynamic forces acting on a vehicle is required. To this end, we perform experiments in a wave tank with an ROV to validate the use of Linear Wave Theory (LWT) to capture the time history of surge, heave and pitch wave induced forces and moments. Validation is performed for various sea states, reconstructed with a mean correlation of 0.9138 in comparison to experimental measurements, displaying a maximum normalised mean error deviation between simulation and experimental data of 0.16 and 0.27 respectively for surge and heave forces, and 0.34 for pitch moment. The effectiveness of employing real-time wave disturbance forecasting for the purpose of anticipatory control is then assessed by incorporating the predicted loads within a Model Predictive Controller. Results display a mean RMS positional error reduction of 47.32% in comparison to a standard PD controller. This presents evidence that accurate, near real-time predictions of the wave-generated forces and moments on an ROV can be produced, laying the foundation for developing model-based predictive control strategies that better suit operation in harsh environments.

**Index Terms**—Marine Robotics, Disturbance Estimation, Motion Control, Model Predictive Control, Station Keeping.

## I. INTRODUCTION

**A** CURRENT trend in the offshore energy industry is the shift towards fully autonomous operation, one aspect of which is the deployment of underwater vehicles for tasks such

as inspection, maintenance and decommissioning of marine renewable energy devices [1], [2]. To reduce the overall operating costs of the plant, accurate sensor deployment and systematic maintenance must be undertaken in a cost-efficient manner through the adoption of relevant technologies [3]–[5]. The oil and gas industry has previously utilised Remotely Operated Vehicles (ROV) for the aforementioned tasks [6], however, they are often not equipped to operate in a more dynamic environment where marine renewable energy devices are commonly situated [7]. In comparison to a deep water scenario with negligible disturbances, performing tasks in these daunting conditions presents situations where strong currents are coupled with high wave energy, which can greatly influence the vehicle behaviour [8].

Evolving from remote to fully autonomous operation gives rise to the particular challenge of accurately estimating the vehicle dynamic response when subjected to external forces and moments, applied to the body by sources such as surface waves or ocean currents [9]. This is particularly necessary for shallow water applications, where the highly dynamic and non-linear nature of the ocean environment makes it critical that disturbance rejection for safe station keeping can be performed to facilitate autonomous operation in close proximity to submerged structures. Typical approaches have either focused on developing methods for disturbance estimation and rejection from *in-situ* observations [10]–[12] as opposed to in a predictive manner, or have focused on rejecting disturbances arising from steady or impulse perturbations rather than wave disturbances [13], [14].

When operating in waves, typical dynamic positioning control aims at filtering out the first order, short timescale component of the wave, while rejecting disturbances from the wave drift component alone [9]. However, for manipulation tasks or visual inspection at close-quarters, both precise positional and attitude control is required for effective station keeping, thus requiring active disturbance rejection of the oscillatory wave component. For this type of control task, classic position/velocity feedback control or even acceleration feedback cannot offer a satisfactory level of performance, especially when exposed to large amplitude, quickly varying disturbances [15]–[17]. This highlights the need for control strategies which incorporate estimation of the highly unsteady disturbance in an anticipatory fashion [18]–[20].

Manuscript received: Feb. 12, 2021; Accepted April 05, 2021.

This paper was recommended for publication by Editor Pauline Pounds upon evaluation of the Associate Editor and Reviewers' comments.

This work was supported by the EPSRC under grant No. EP/R026173/1 and grant No. EP/R513209/1.

<sup>1</sup>Kyle L. Walker, Simona Aracri, Adam A. Stokes and Francesco Giorgio-Serchi are with the Institute for Integrated Micro and Nano Systems, School of Engineering, University of Edinburgh, Edinburgh, U.K. (Correspondence: F.Giorgio-Serchi@ed.ac.uk).

<sup>2</sup>Roman Gabl is with the FloWave Ocean Research Facility, School of Engineering, University of Edinburgh, Edinburgh, U.K.

<sup>3</sup>Yu Cao and Aristides Kiprakis are with the Institute for Energy Systems, School of Engineering, University of Edinburgh, Edinburgh, U.K.

<sup>4</sup>Simona Aracri is also with the Institute for the Study of Anthropogenic Impacts and Sustainability in Marine Environment (IAS), National Research Council (CNR), Genova, Italy.

Digital Object Identifier (DOI): see top of this page.

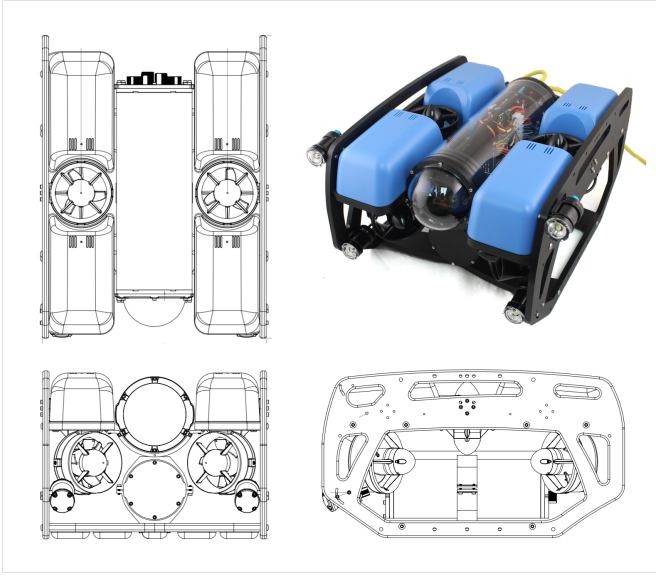


Fig. 1: The BlueRobotics BlueROV2, [26].

Fast prediction of fluid forces on submerged bodies is commonly performed via potential flow-based approximations. One such example broadly employed for bodies operating in waves is represented by Response Amplitude Operators (RAOs), which are used extensively for studying the force and motion response of complex geometries in the frequency domain [16]. Similarly, by approximating the body shape to elementary geometrical units and relying on suitable coefficients for the hydrodynamic parameters, Linear Wave Theory (LWT) can provide an estimate of local flow features, thus enabling a solution of the body dynamics in the time domain. While this approach has been employed extensively for design practice [21], it also lends itself to employment for control purposes due to its very limited computational cost. Nonetheless its usage in real-time disturbance prediction for the purpose of feed-forward control remains sparse and its real applicability uncertain.

Following this approach, in this letter the external forces and torques induced by a dynamically changing sea state acting on an ROV are simulated and validated against data collected during an experimental study conducted at the FloWave Ocean Energy Research Facility, University of Edinburgh [22], [23]. These estimations are then implemented within a Model Predictive Controller to simulate a station keeping scenario, drawing performance comparisons with a PD controller. The results aim to demonstrate the degree of accuracy which can be achieved with a low-order model in capturing the vehicle dynamics in highly-perturbed, wave-dominated environments and through this, justify the employment of such models for the purpose of predictive control in such scenarios.

## II. THEORETICAL MODELLING

This section details the underlying theory and approximations which are applied to obtain an estimate of the hydrodynamic forces acting on the vehicle due to the surface activity.

TABLE I: BlueROV2 dimensions and hydrodynamic parameters utilised in the simulations; data based on [25]–[27].

Parameter	Nomenclature	Value
Density of Seawater	$\rho$	$1025 \text{ kg/m}^3$
Dry Mass	$m_d$	$11 \text{ kg}$
Vehicle Length	$l$	$457 \text{ mm}$
Vehicle Width	$b$	$338 \text{ mm}$
Vehicle Height	$h$	$254 \text{ mm}$
Rotational Inertia, $q$	$I_{yy}$	$0.16 \text{ kgm}^2$
Added Mass, $x$	$X_{\dot{u}}$	$5.5 \text{ kg}$
Added Mass, $z$	$Z_{\dot{w}}$	$14.57 \text{ kg}$
Added Mass, $q$	$M_{\dot{q}}$	$0.12 \text{ kgm}^2/\text{rad}$
Restoring Moment Arm, $q$	$\overline{BG}_z$	$0.02 \text{ m}$
Maximum Output Thrust	$T_{max}$	$40 \text{ N}$
Thruster Angle, $x$	$\alpha_1, \alpha_2, \alpha_3, \alpha_4$	$45^\circ$

The simulated scenario is modelled in conjunction with the parameters of the experiments detailed in Section III.

### A. Vehicle Dynamics

The ROV is modelled as a rigid, neutrally buoyant body. The concerned Degrees of Freedom (DOF) are the surge, heave and pitch, as this work concerns 2D planar waves and the disturbances induced in the same plane. Using SNAME notation, the vehicle dynamics in these 3DOF (surge, heave and pitch) can be represented by:

$$m_d[\dot{u} + wq - x_G q^2 + z_G \dot{q}] = X_{\dot{u}} \dot{u} + X_{\dot{w}}(\dot{w} + uq) + X_{\dot{q}} \dot{q} + Z_{\dot{w}} wq + Z_{\dot{q}} q^2 + X_{u|u}|u| - (W - B) \sin \theta + T_x \cos \theta + T_z \sin \theta \quad (1)$$

$$m_d[\dot{w} - uq + x_G \dot{q} + z_G q^2] = Z_{\dot{w}} \dot{w} + X_{\dot{w}}(\dot{u} - wq) + Z_{\dot{q}} \dot{q} - X_{\dot{u}} uq - X_{\dot{q}} q^2 + Z_{w|w}|w| + (W - B) \cos \theta + T_z \cos \theta + T_x \sin \theta \quad (2)$$

$$I_{yy} \dot{q} + m_d[z_G(\dot{u} + wq) - x_G(\dot{w} - uq)] = X_{\dot{q}}(\dot{u} + wq) + Z_{\dot{q}}(\dot{w} - uq) + M_{\dot{q}} \dot{q} - X_{\dot{w}}(u^2 - w^2) - (Z_{\dot{w}} - X_{\dot{u}})uw + M_{q|q}|q| + M_{w|w}|w| - \overline{BG}_z W \sin \theta + \delta T_z \quad (3)$$

where  $u$  and  $w$  represent the relative velocities between the local flow speed and the vehicle, such that:

$$u = u_p - u_v, \quad w = w_p - w_v$$

where subscript  $p$  and  $v$  represent the fluid particle and vehicle velocity, respectively. Also,  $T$ ,  $\overline{BG}_z$ ,  $W$ ,  $B$  and  $\delta$  are the thrust produced by the propellers, the vector between the centre of gravity and centre of buoyancy in the heave, the vehicle dry weight, the vehicle buoyancy and the moment arm to the vertical thrusters, respectively. The terms  $X_{\dot{u}}$ ,  $Z_{\dot{w}}$ ,  $X_{u|u}$ ,  $Z_{w|w}$  represent the linear added mass and viscous damping coefficients, while  $M_{\dot{q}}$ ,  $M_{q|q}$  are the coefficient of rotational drag and added moment of inertia for the pitch. The restoring moment is also considered in the pitch dynamics. The physical parameters of the simulation and the BlueROV2 are displayed in Table I following data from [25], [26].

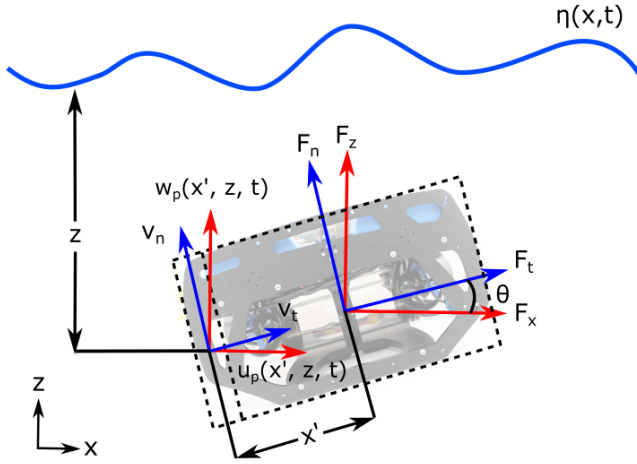


Fig. 2: Particle velocities and resultant forces acting on the vehicle in both the local and global co-ordinate frame, depicting the different components acting along the vehicle longitudinal axes with reference to the vehicle pitch,  $\theta$ .

### B. Wave-induced flow prediction

Estimation of  $u_p$  and  $w_p$  is based on LWT, according to which the time history of the sea elevation  $\eta(x, t)$  at a prescribed location can be represented as a composition of  $N$  monochromatic waves [24] of known wave height,  $H$ , period,  $T$ , and phase offset,  $\phi$ , thus yielding:

$$\eta(x, t) = \sum_{i=1}^N \frac{H_i}{2} \cos(k_i x - \omega_i t + \phi_i) \quad (4)$$

where  $k$ ,  $\omega$  and  $\lambda$  represent the wave number, the angular frequency and the wavelength.

Knowledge of these characteristics for each wave component facilitates the reconstruction of the local flow field in the whole domain [8]:

$$u_p(x, z, t) = \sum_{i=1}^N \frac{\pi H_i}{T_i} \frac{\cosh k(z+d)}{\sinh kd} \cos(k_i x - \omega_i t + \phi_i) \quad (5)$$

$$w_p(x, z, t) = \sum_{i=1}^N \frac{\pi H_i}{T_i} \frac{\sinh k(z+d)}{\sinh kd} \sin(k_i x - \omega_i t + \phi_i) \quad (6)$$

where  $z$  and  $d$  are the operating depth of the vehicle and total depth of the water column respectively.

### C. Wave-induced hydrodynamic loads prediction

Estimation of quadratic drag and inertial fluid forces on the vehicle is straight forward, as the forces are considered as a simple superposition [9]. However, computation of the moment exerted by the wave on the vehicle requires an *ad-hoc* treatment, since it requires consideration of force variation over the body. In consideration of the need for fast prediction, a low-order integration of the hydrodynamic forces over the sagittal plane of the vehicle is employed. Whilst this approach stretches the validity of slender-body theory in the case of an ROV, it enables a degree of prediction within a time frame suitable for real-time control.

TABLE II: Experimental parameters for the test cases considered. For monochromatic cases R01 - R03, the peak frequency refers to the wave frequency.

Case Reference	Significant Wave Height (m)	Peak Frequency (Hz)
R01	0.1	0.5
R02	0.2	0.5
R03	0.4	0.5
JS01	0.2	0.5
JS02	0.4	0.5
JS03	0.6	0.5

Having defined  $x'$  and  $z'$  the body-fixed coordinates of the vehicle, we refer to  $v_t$  and  $v_n$  as the flow velocity components tangential and normal to the vehicle, computed by projection of  $v_t$  and  $v_n$  along the local coordinates, see Fig. 2. We assume the vehicle can be treated as a set of identical sections with the same hydrodynamic properties, thus the local Morrison force exerted on an infinitesimal section of the vehicle's  $x'$  axis can be defined as:

$$F(x', t) = \rho V \dot{v}_n(x', t) + \rho C_a V \dot{v}_n(x', t) + \frac{1}{2} \rho C_d A_i v_n(x', t) |v_n(x', t)| \quad (7)$$

where  $V$  is the spanwise volume of the section,  $C_a$  is the added mass coefficient,  $C_d$  is the drag coefficient and  $A_i$  is the section incident area to the flow. The above correlates with Eq. 3, such that the resulting moment can be expressed as the integral along  $x'$ , producing:

$$M_{\dot{q}} \dot{q} + M_{q|q} q|q| = \int_{-\frac{L}{2}}^{\frac{L}{2}} F(x', t) x' dx' \quad (8)$$

where  $L$  is the vehicle longitudinal length. This methodology presents a basis for theoretically evaluating the resulting moment due to a non-constant flow arising from fluctuations at the sea surface. For the pitching of the vehicle, only the normal force acting on the vehicles local heave plane was considered to be sufficiently contributing to this motion.

### D. Thrust Allocation

The BlueROV2 features six vectored thrusters, 4 horizontal and 2 vertical and is controllable in 5 DOF, the pitch being the only uncontrollable plane, see Fig. 1. If we consider the bilinear model,  $\tau = \mathbf{B}\boldsymbol{\mu}$ , where  $\mathbf{B}$  is an allocation matrix and  $\boldsymbol{\mu}$  is a vector of control inputs; the applied forces and moments from the thrusters can be deduced from their specifications and geometries in the vehicle's local co-ordinate frame [9]. As the surge and heave are the two controllable planes in this letter, the vector of output thrusts is summarised as:

$$\boldsymbol{\tau} = \begin{bmatrix} T_x \\ T_z \end{bmatrix} = T_{max} \begin{bmatrix} c\alpha_1 & c\alpha_2 & c\alpha_3 & c\alpha_4 & 0 & 0 \\ 0 & 0 & 0 & 0 & 1 & 1 \end{bmatrix} \boldsymbol{\mu} \quad (9)$$

where  $c$  is shorthand for  $\cos$ , the angles  $\alpha_1 - \alpha_4$  are the horizontal thruster orientation with respect to the vehicle's local  $x$ -axis and  $\boldsymbol{\mu} = \{\mu_1, \mu_2, \mu_3, \mu_4, \mu_5, \mu_6\}^T$ . This model can be implemented within the simulation for evaluating the station keeping performance of different control architectures.

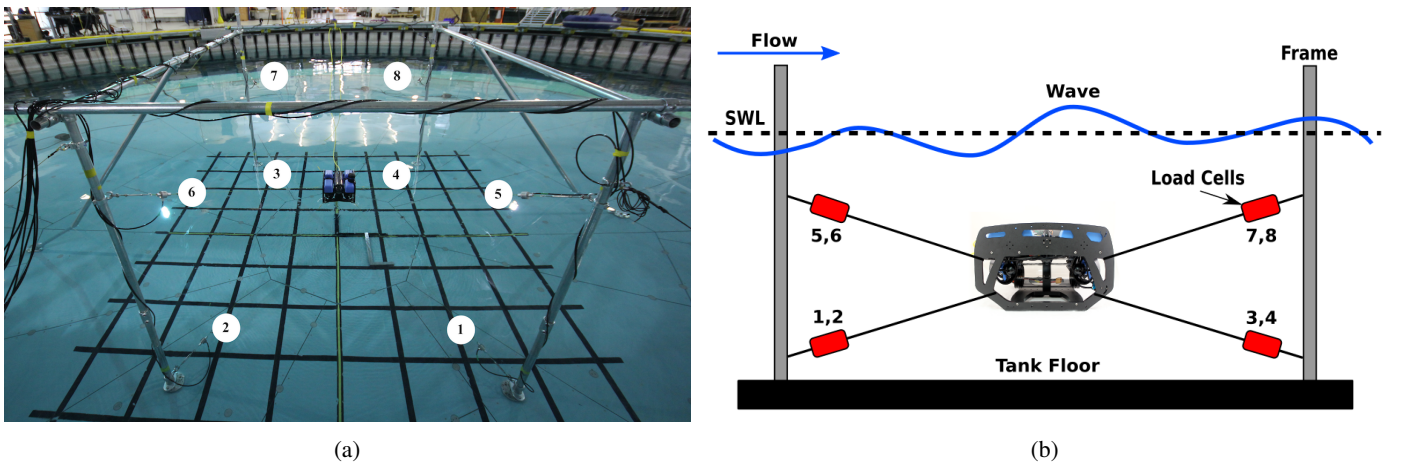


Fig. 3: Experimental set-up used for collecting data, visualising the position of the load cells with their respective assignments and how the vehicle was restrained within the frame, with reference to the Still Water Line (SWL). Fig. 3a shows an image of the actual apparatus within FloWave (raised tank floor) and Fig. 3b schematically describes the arrangement, with the load cell number assignments shown.

### III. EXPERIMENTAL PROCEDURE

To facilitate validation of the estimated hydrodynamic forces, experimental data was collected during an investigation at the FloWave facility, University of Edinburgh. The vehicle utilised in this work was the BlueROV2 produced by Blue Robotics, a small scale ROV who's physical and hydrodynamic parameters are displayed in Table I [25], [26].

The BlueROV2 was restrained within a purpose-built frame by eight tethers to minimise interference of the supporting structure with the flow around the ROV. Each tether was fitted with an in-line load cell to measure the force exerted on the body by the wave, as shown schematically in Fig. 3. The upper volume of the wave tank has a total depth of 2m and a diameter of 25m, with the vehicle situated in the centre at 1m depth for all experiments. The vehicle was subjected to varying degrees of wave disturbances created by the surrounding wave makers and the force acting on the vehicle was monitored, as well as any very small motions in 6DOF evaluated based on a Qualisys underwater motion capturing system. The disturbances are generated by specifying the parameters of the frequency spectrum, which is then transformed into a wave height time-history; this is transferred to the wave-makers, resulting in movement to produce the desired waveform. The test case conditions are listed with assigned case references in Table II. The load cells measure the inline force vector, which can be decomposed into the individual 3-dimensional force components by considering the geometrical arrangement of the apparatus. The force vector orientation was determined based on two points (one on the frame and a virtual one calculated based on the rigid body of the ROV), measured with the underwater motion capturing system to an accuracy within the range of 1mm. This processed data [30] was used for validation against the estimated forces presented in this work. Each load cell is assigned a number for ease of analysis, ranging from LC1 up to LC8, shown in the experimental apparatus in Fig. 3. Further information

regarding the collected data, processing of the data and the full experimental procedure can be found in [28].

Within the simulations, it was assumed that the vehicle remained perfectly stationary and the oncoming wave was assumed to be a perfect head sea. When the waves are generated in the FloWave Facility, a wave-height time history is created by the software and passed to the wave makers. It was possible to extract this time history for all experiments; therefore, Fourier analysis could be used to obtain the frequency components and their attributes ( $H$ ,  $T$  and  $\phi$ ) to reconstruct each case in simulation, applying the theory detailed in Section II-B. The simulations were performed by implementing a fifth-order Runge-Kutta integration [29] to solve the differential equations presented in Section II; each case was simulated for a total of 300s and compared with the corresponding experimental data. The complete processed dataset for the conducted experiments is available via the DataShare of the University of Edinburgh [30].

### IV. RESULTS

Comparing the measurements with the experimental data for the surge force, heave force and pitching moment (based on the previous observations) presents an impression of how realistic the simulation is. For all cases, the sea state created by the wave makers was emulated; for the irregular cases, Fourier analysis was utilised to identify the JONSWAP frequency components as previously mentioned. From these frequency components, the sea state was reconstructed and the hydrodynamic forces estimated according to LWT; a section of the time histories for the fully developed wave in cases R02 and JS01-JS03 are depicted in Fig. 4-7. These show good correlation between the estimations and the experimentally collected data, demonstrating that the lower order model can provide a fair representation of the particle motions and resulting forces induced by surface waves. It should be noted that a Savitzky-Golay filter was applied to the experimental data to smooth the signal and reduce the amount of sensor noise; however,

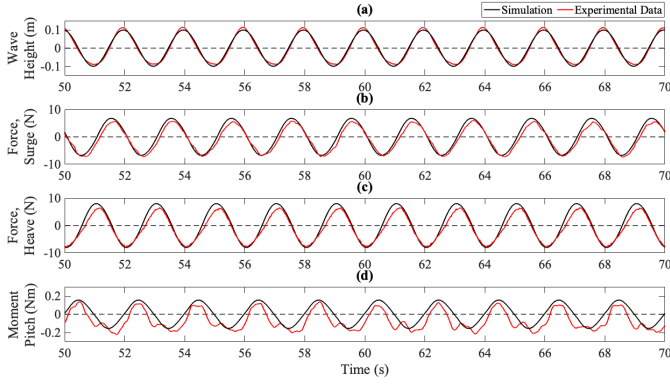


Fig. 4: Comparison between simulation and experimental data for case R02, showing the time segment 50s - 70s. The subplots display the (a) wave height, (b) surge force, (c) heave force and (d) pitching moment.

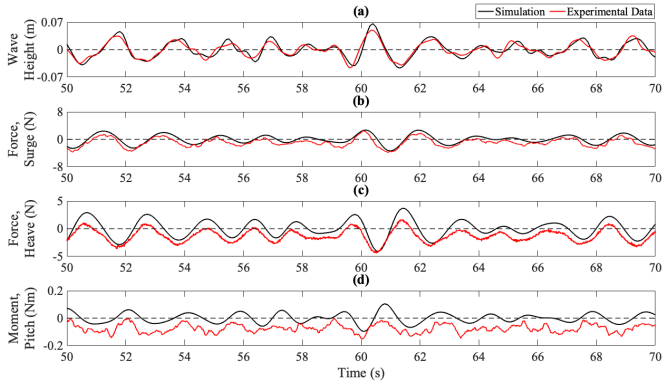


Fig. 5: Comparison between simulation and experimental data for case JS01, showing the time segment 50s - 70s. The subplots display the (a) wave height, (b) surge force, (c) heave force and (d) pitching moment.

all plots still show some effect of noise on the resulting trace. This is mainly due to 2 of the load cells being rated higher, causing low magnitude wave elevations to be affected by a higher degree of background sensor fluctuation [28]. There may also be components operating at a frequency similar to that of the wave associated with the frame and measurement gauges, which are difficult to segregate from the force signal. Furthermore, the motion capturing system documented very small rotations and translations, which are not reproduced in the LWT approach due to the assumption of a perfect still geometry. However, the overall behaviour can still be seen as consistent, particularly for case JS03 where the significant height is largest.

Further analysis was conducted regarding the statistical similarity between the simulated data and the experimental data. The data is graphically represented in Fig. 8, which again demonstrates that the distribution of the data matches well for all cases. Expanding this analysis further, the normalised error for all test cases are shown in Fig. 9; for the four variables considered here (wave height, surge/heave force and pitching moment), the correlation factors were

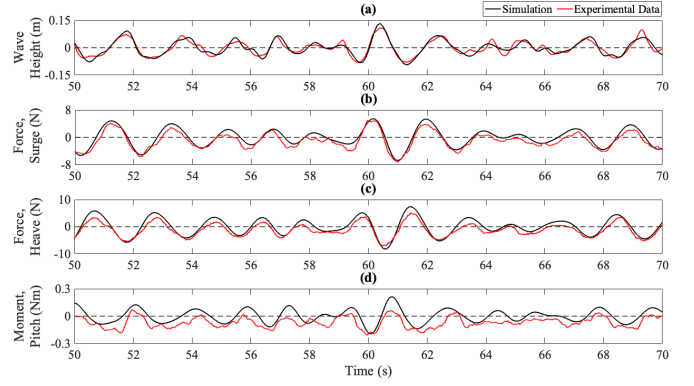


Fig. 6: Comparison between simulation and experimental data for case JS02, showing the time segment 50s - 70s. The subplots display the (a) wave height, (b) surge force, (c) heave force and (d) pitching moment.

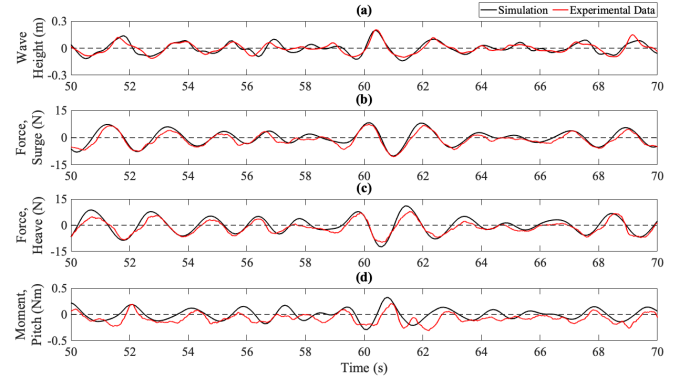


Fig. 7: Comparison between simulation and experimental data for case JS03, showing the time segment 50s - 70s. The subplots display the (a) wave height, (b) surge force, (c) heave force and (d) pitching moment.

also obtained to offer further quantitative insight into the simulation/experiment comparison, listed in Table III. This additional analysis presents insight into the deviation of the estimated forces with reference to the real-world case.

Finally, to demonstrate the applicability of the force estimation, we conclude our results with a station keeping performance comparison between a classic PD control and Model Predictive Control (MPC); the key parameters associated with both controllers can be found in Table IV. The objective of this comparison is to demonstrate the potential performance improvement through inclusion of wave disturbances within the control scheme. For the PD controller, the control inputs are determined according to the control law defined by:

$$\mu(t) = K_p e(t) + K_d \frac{de(t)}{dt} \quad (10)$$

where  $K_p$ ,  $K_d$  and  $e$  are the proportional gain, derivative gain and positional error respectively.

Alternatively, the MPC objective is to minimise the cost function,  $J$ , for the sum of squared distances between the

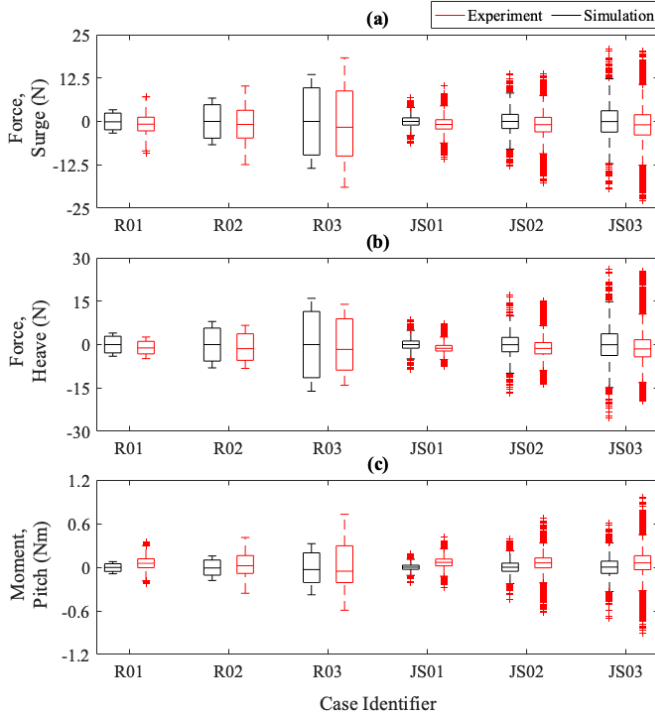


Fig. 8: Boxplot distribution comparing the simulated data to the experimentally collected data. The plots display the median, the interquartile range (IQR), outliers (points which fall  $\geq 1.5 \times$  IQR above the third quartile or below the first quartile, individually marked by a '+') and whiskers extending to the most extreme data points not considered outliers by mathematical definition.

desired state,  $\Lambda_d$ , and the predicted state,  $\Lambda_j$  [19]:

$$J = \sum_{j=1}^K \{ \Lambda_d - \Lambda_j(\mu_j) \}^2 + (\mu_j)^2 \quad (11)$$

where  $K$  is the horizon length,  $j$  is the current time step and the term  $(\mu_j)^2$  is intended to minimise energy usage. The control inputs are constrained such that  $-1 \leq \mu \leq 1$  as the output thrust cannot exceed the maximum attainable, as described by Eq. 9. Subsequently evaluating the Jacobian with respect to the control input determines the optimised values for the control vector  $\mu$ .

This analysis concerned cases JS01-JS03, where the vehicle was subjected to the surface waves and the controller attempted to hold the vehicle position at  $(0, -1)$  m, mimicking the experimental conditions; as with our previous analysis, the simulations were performed for 300s, see Fig. 10 which depicts an example for case JS03 (showing only 0-60s for clarity), providing clear evidence that inclusion of disturbance estimations greatly improves the vehicles station keeping ability. Across all cases there was a mean reduction in Root Mean Squared (RMS) error of 47.32%, with the explicit RMS errors shown in Fig. 11.

## V. DISCUSSION

Upon reflection of the results detailed in Section IV, it is shown that the modelled theory accurately represents the

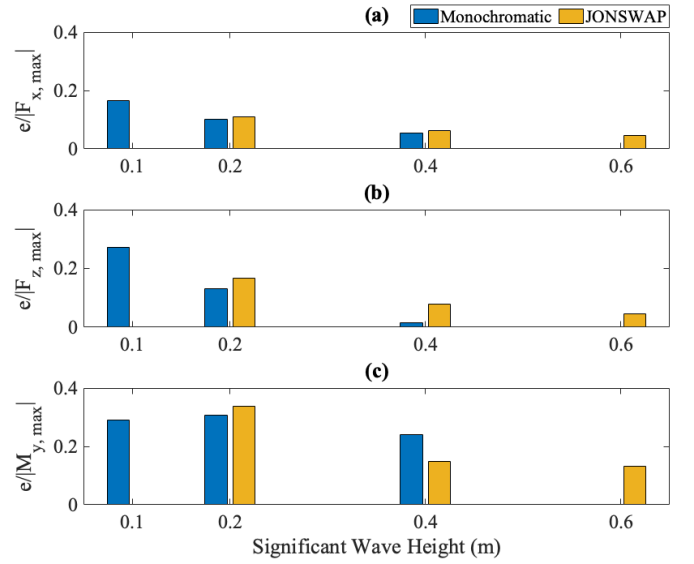


Fig. 9: Normalised mean error magnitude for each case, relative to the maximum force recorded throughout the duration of the case relative to the significant height of the wave train.

hydrodynamic forces under varying conditions. These results show that LWT is capable of closely matching a wave profile consistent with a complex wave series, such as that produced by the wave makers. With reference to Fig. 8, the moment value, Fig. 8(c), displays the largest deviation in range between the datasets, which correlates with the results displayed in Fig. 9; this suggests that the angular torques feature higher uncertainty. Due to the error analysis being a timewise point-to-point comparison, there will be occasions where the lower-order model and the experimental data largely differ, which will produce a larger error range, as demonstrated in Fig. 9. However, the overall model output closely follows the unsteady behaviour of the systems with remarkable accuracy, with the majority of the data falling within a small normalised

TABLE III: Correlation coefficients between the estimated forces and the experimental data for the wave height,  $\eta$ , surge force,  $F_x$ , heave force,  $F_z$  and pitching moment,  $M_\theta$ .

Variable	Case					
	R01	R02	R03	JS01	JS02	JS03
$\eta$	0.9671	0.9423	0.8484	0.9403	0.9259	0.8585
$F_x$	0.925	0.9811	0.7207	0.9349	0.9661	0.9459
$F_z$	0.9205	0.9882	0.6567	0.9688	0.9707	0.9317
$M_\theta$	0.8728	0.8796	0.4570	0.6571	0.7637	0.6402

TABLE IV: Controller parameters for the PD and MPC controllers utilised for comparing station keeping performance, exclusive and inclusive of disturbance prediction.

Controller	Parameter	Nomenclature	Value
PD	Proportional Gain	$K_{p,x}, K_{p,z}$	1.4, 1.8
	Derivative Gain	$K_{d,x}, K_{d,z}$	2.7, 3.2
MPC	Prediction Horizon	$t_p$	0.8s
	Prediction Steps	$\Delta t$	4

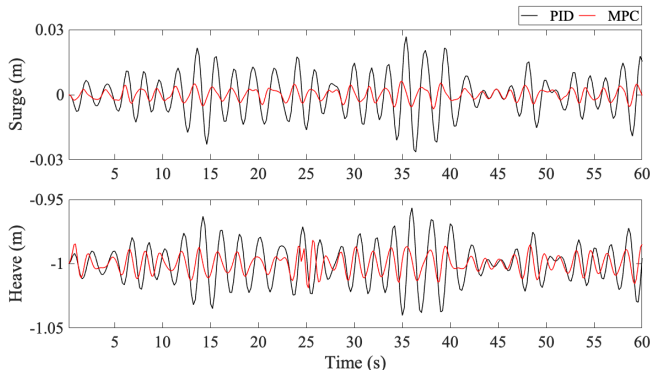


Fig. 10: Station keeping performance using a PD controller vs a Model Predictive Controller, when operating under the wave train in case JS03 and attempting to station keep at the position  $(0, -1)m$ .

error range. It can also be seen that the mean error is slightly positive, which could indicate some experimental errors, supported by a slight constant y-offset witnessed in Fig. 4-7, particularly Fig. 5. For all cases, the normalised mean error recorded is  $< 0.35$  showing that the model is a fair general representation of the wave induced forces and moments. This is supported by the correlation factors listed in Table III, which are close to 1 for all parameters across the majority of cases.

One factor which contributes to the error is the assumption that the vehicle is held perfectly stationary and oriented perfectly head-on to the oncoming wave. However, unwanted small-scale displacements of the vehicle during the experiments were inevitable, yielding an unavoidable mismatch with the simulated case-scenario. Additionally, within the simulation only the forces arising from the added mass and viscous damping effects are considered and other forces, such as the Froude-Krylov force for example, are disregarded.

Considering the apparatus, the restraining cables were chosen as inextensible lightweight Dyneema rope; however, there will still be an effect on the recorded moment due to the vehicle not being held perfectly stationary. Additionally, it's possible that imperfect pre-tensioning or momentaneous misalignment of the supporting rig will cause discrepancies, as these could allow room for some unwanted small angular motions. This could be the reason that the comparison of recorded and simulated moments in Fig. 4(d)-7(d) do not match as closely as the linear forces, but the overall behaviour exhibited still shows good consistency. This could also account for the offset witnessed in the recorded moment, which appears to be shifted slightly for all cases tested; if the vehicle is not orientated perfectly head on to the wave throughout the entire experiment, additional contributions will be present in the measured forces which were not accounted for within the simulation, thus affecting the accuracy of our results.

A clear factor effecting the correlation is that the emulated wave is not an identical match to the wave generated by the wave makers; the experimental case will feature imperfections and this will therefore cause deviations before any approximations are even considered. Limitations of LWT make it applicable only under various assumptions, such as the wave

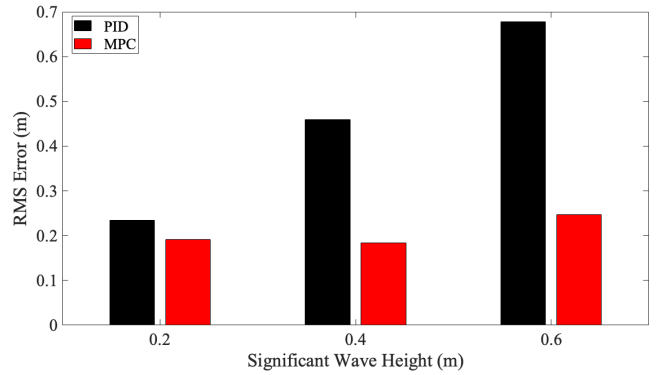


Fig. 11: Associated RMS errors for cases JS01 - JS03 over a 300s simulation, showing a mean reduction of 47.32% when using Model Predictive Control over PD control.

steepness ( $H/\lambda$ ) remaining small and the sea floor having negligible impact on the sinusoidal nature of the wave. While these are satisfied for the cases tested and for a broad range of real-world scenarios, the validity of these assumptions will be stretched for waves which diverge from a pure swell [24].

Looking at the improved performance using MPC, there is a substantial reduction in RMS error for all tested cases; 18.58% for  $H_s = 0.2m$ , 59.92% for  $H_s = 0.4m$  and 63.46% for  $H_s = 0.6m$  which was the largest significant wave height tested. Although promising, these results were achieved when assuming full knowledge of the wave spectrum at the vehicle's location had been achieved through the prediction algorithm. Also, the thrust delivered was assumed to not suffer from any time delay, analogous to [19], while it can be expected that even small time lag in the thrust response signal can significantly affect controller performance [17].

With reference to the above, the estimated forces validated in this letter present a good approximation in comparison to those measured during the experiments. These estimations provide an understanding of the dynamic response of the vehicle subject to surface wave disturbances, and were shown to improve performance when incorporated into controller design, specifically for tasks such as station keeping in harsh environments. Furthermore, the model not only captures the complex dynamics with good accuracy but computes the hydrodynamic forces at a speed applicable for real-time applications (a 20s time history is analysed in  $\approx 5s$  using MATLAB on a laptop with a 1.6GHz Dual-Core Intel Core i5 processor), strengthening the case for use in dynamic control applications.

## VI. CONCLUSION

This letter presents experimental validation of the estimation of hydrodynamic forces acting on an ROV under regular and irregular waves of different significant heights. The resulting estimations have been subject to both qualitative and quantitative analysis, which has shown that the employed low-order model provides a good degree of accuracy at very limited computation cost. With reference to the irregular sea states tested, the wave elevation was consistently captured with a mean correlation factor of  $\approx 0.9$ , while the associated surge

and heave forces were predicted with a mean correlation factor of 0.95 and 0.96 respectively. The model accurately forecasts the variation of these linear forces throughout the experiments, closely matching their spreading over the median and interquartile range, predicting the measured signal with a normalised mean error smaller than 0.17, see Fig. 9. Prediction of the hydrodynamic pitching moment, despite requiring a coarse piecewise integration, correlated with the measured data with a 0.69 factor when averaged over the irregular cases. The normalised mean error between experimental data was consistently below 0.35, and fell below 0.14 for the largest significant wave height tested. The model can also be executed at a speed which suggests it is applicable for real-time applications.

To prove that low-order models can be deployed as predictive tools for both positional and attitude control, the estimates from the model were incorporated within a predictive control architecture, ultimately showing station keeping performance was improved between 18-63% across different sea states compared to a typical PD controller. To further investigate our approach, future work will focus on expanding our analysis by considering multi-directional spectra to determine the performance of our proposed system in a scenario analogous to real-world environments. While significant improvements are essential to successfully employ predictive control tools in real-world applications, these results constitute a solid foundation upon which the challenge of autonomous operation in harsh ocean environments can be addressed.

## REFERENCES

- [1] R. Capocci, E. Omerdic, G. Dooly and D. Toal, "Development and Testing of Remotely Operated Vehicles for Inspection of Offshore Renewable Devices", in *IFIP Advances in Information and Communication Technology*, vol. 521, pp. 282–289, 2018.
- [2] S. Sivčev, E. Omerdić, G. Dooly, J. Coleman and D. Toal, "Towards inspection of marine energy devices using ROVs: Floating wind turbine motion replication," in *Advances in Intelligent Systems and Computing*, vol. 693, Springer Verlag, pp. 196–211, 2018.
- [3] E. Omerdic, D. Toal, G. Dooly and A. Kaknjo, "Remote presence: Long endurance robotic systems for routine inspection of offshore subsea oil & gas installations and marine renewable energy devices", in *Proceedings of OCEANS 2014 MTS/IEEE*, St. John's, NL, Canada, 2014.
- [4] M. Sayed, M. Nemitz, S. Aracri, A. McConnell, R. McKenzie and A. Stokes, "The Limpet: A ROS-Enabled Multi-Sensing Platform for the ORCA Hub", *Sensors*, vol. 18, no. 10, p. 3487, Oct. 2018.
- [5] F. Remouit, "Automation of underwater operations on wave energy converters using remotely operated vehicles", Ph.D. Thesis, *Faculty of Science and Technology*, Uppsala Universitet, Sweden, 2018.
- [6] D. Khojasteh and R. Kamali, "Design and dynamic study of a ROV with application to oil and gas industries of Persian Gulf," *Ocean Engineering*, vol. 136, pp. 18-30, May 2017.
- [7] E. Rusu and F. Onea, "A review of the technologies for wave energy extraction", *Clean Energy*, vol. 2, no. 1, pp. 10–19, 2018.
- [8] D. Reeve, A. Chadwick, and C. Fleming, "Coastal Engineering: Processes, Theory and Design Practice", *Spon Press*, 2004.
- [9] T. I. Fossen, "Guidance and control of ocean vehicles," *Wiley*, 1994.
- [10] J. Riedel and A. Healey, "Shallow Water Station Keeping of AUVs Using Multi-Sensor Fusion for Wave Disturbances Prediction and Compensation", in *Proceedings of OCEANS 1998 MTS/IEEE*, Nice, France, pp. 1064-1068, 28 Sept. - 01 Oct. 1998.
- [11] J. Kim, H. Joe, S. Yu, J. S. Lee and M. Kim, "Time-Delay Controller Design for Position Control of Autonomous Underwater Vehicle Under Disturbances", in *IEEE Transactions on Industrial Electronics*, vol. 63, no. 2, pp. 1052-1061, Feb. 2016.
- [12] Y. Zhang and L. Wang, "Real-Time Disturbances Estimating and Compensating of Nonlinear Dynamic Model for Underwater Vehicles", *Mathematical Problems in Engineering*, 2018.
- [13] J. Guerrero, J. Torres, V. Cuezue and A. Chemori, "Adaptive Disturbance Observer for Trajectory Tracking Control of Underwater Vehicles", *Ocean Engineering*, vol. 200, Feb. 2020.
- [14] J. M. Selvakumar and T. Asokan, "A Novel Approach to Measure under Water Vehicle Disturbance Force for Station Keeping Control", in *Proceedings of the 9th International Conference on Informatics in Control, Automation and Robotics (ICINCO)*, Rome, Italy, pp. 460–463, July 28-31 2012.
- [15] K. L. Walker, A. A. Stokes, A. Kiprakis, and F. Giorgio-Serchi, "Investigating PID Control for Station Keeping ROVs", in *Proceedings of UKRAS20 Conference: "Robots into the real world"*, Lincoln, U.K., pp. 51–53, 17th April 2020.
- [16] H. S. Halvorsen, H. Øveraas, O. Landstad, V. Smines, T. I. Fossen, T. A. Johansen, "Wave motion compensation in dynamic positioning of small autonomous vessels", *Journal of Marine Science and Technology*, 2020.
- [17] K. L. Walker, A. A. Stokes, A. Kiprakis, and F. Giorgio-Serchi, "Impact of Thruster Dynamics on the Feasibility of ROV Station Keeping in Waves", in *Proceedings of OCEANS 2020 MTS/IEEE, Singapore - U.S. Gulf Coast*, October 5th - 30th 2020. *In Press*.
- [18] P. Walters, R. Kamalapurkar, F. Voight, E. M. Schwartz and W. E. Dixon, "Online Approximate Optimal Station Keeping of a Marine Craft in the Presence of an Irrotational Current", *IEEE Transactions on Robotics*, vol. 34, no. 2, pp. 486–496, 2018.
- [19] D. C. Fernandez and G. A. Hollinger, "Model Predictive Control for Underwater Robots in Ocean Waves", *IEEE Robotics and Automation Letters*, vol. 2, no. 1, pp. 88–95, 2017.
- [20] V. T. Huynh, M. Dunbabin and R. N. Smith, "Predictive motion planning for AUVs subject to strong time-varying currents and forecasting uncertainties", in *Proceedings of IEEE International Conference on Robotics and Automation (ICRA)*, Seattle, WA, USA, pp. 1144–1151, 26 May - 30 May 2015.
- [21] Michael E. McCormick, "Ocean Engineering Mechanics with Applications, *Cambridge University Press*, Cambridge, 2009.
- [22] D. Ingram, R. Wallace, A. Robinson and I. Bryden, "The design and commissioning of the first, circular, combined current and wave test basin", in *Proceeding of OCEANS 2014 MTS/IEEE*, Taipei, Taiwan, pp. 15–29, 7-10 April 2014.
- [23] S. Draycott, B. Sellar, T. Davey, D. R. Noble, V. Venugopal and D. M. Ingram, "Capture and simulation of the ocean environment for offshore renewable energy", *Renewable Sustainable Energy Reviews*, vol. 104, pp. 15–29, Apr. 2019.
- [24] R. G. Dean and R. A. Dalrymple, "Water wave mechanics for engineers and scientists.", 2nd Edition, *World Scientific*, 1984.
- [25] A. Manzanilla, S. Reyes, M. Garcia, D. Mercado and R. Lozano, "Autonomous navigation for unmanned underwater vehicles: Real-time experiments using computer vision", *IEEE Robotics and Automation Letters*, vol. 4, no. 2, pp. 1351–1356, Apr. 2019.
- [26] Blue Robotics, "BlueROV2: The World's Most Affordable High-Performance ROV", BlueROV2 datasheet, June 2016 [Revised June 2019].
- [27] CJ. Wu, "6-DoF Modelling and Control of a Remotely Operated Vehicle", M.Eng. Thesis, *College of Science and Engineering*, Flinders University, July 2018.
- [28] R. Gabl, T. Davey, Y. Cao, Q. Li, B. Li, K. L. Walker, F. Giorgio-Serchi, S. Aracri, A. Kiprakis, A. A. Stokes and D. M Ingram, "Experimental Force Data of a Restrained ROV under Wave and Current", *Data*, vol. 5, no. 3, p. 57, 2020.
- [29] L. F. Shampine and M. W. Reichelt, "The MATLAB ODE Suite", *SIAM Journal on Scientific Computing*, vol. 18, pp. 1–22, 1997.
- [30] R. Gabl, T. Davey, Y. Cao, Q. Li, B. Li, K. L. Walker, F. Giorgio-Serchi, S. Aracri, A. Kiprakis, A. A. Stokes and D. M Ingram, Dataset "Experimental Force Data of a hung up ROV under Wave and Current", *DataShare Edinburgh* [Dataset], University of Edinburgh, Institute for Energy Systems: Edinburgh, UK, 2020.